HHS Public Access

Author manuscript

Nat Microbiol. Author manuscript; available in PMC 2022 July 15.

Published in final edited form as:

Nat Microbiol. 2020 September ; 5(9): 1088–1095. doi:10.1038/s41564-020-0735-8.

Nuclear pore blockade reveals HIV-1 completes reverse transcription and uncoating in the nucleus

Adarsh Dharan[1], **Niklas Bachmann**[1], **Sarah Talley**[2], **Virginia Zwikelmaier**[1], **Edward M. Campbell**[1,2,*]

[1]Department of Microbiology and Immunology, Stritch School of Medicine, Loyola University, Chicago, USA

[2]Integrative Cell Biology Program, Stritch School of Medicine, Loyola University, Chicago, USA

Abstract

Retroviral infection involves the reverse transcription of the viral RNA genome into DNA, which is subsequently integrated into the host cell genome. HIV-1 and other lentiviruses are able to mediate the infection of non-dividing cells through the ability of the capsid (CA) protein [1] to engage the cellular nuclear import pathways of the target cell and mediate their nuclear translocation through components of the nuclear pore complex (NPC) [2–4]. Although recent studies have observed the presence of capsid in the nucleus during infection[5–8], reverse transcription and disassembly of the viral core have conventionally been considered to be cytoplasmic events. Here, we use an inducible nuclear pore blockade to monitor the kinetics of HIV-1 nuclear import and define the biochemical staging of these steps of infection. Surprisingly, we observe that nuclear import occurs with relatively rapid kinetics (<5 hours) and precedes the completion of reverse transcription in target cells, demonstrating that reverse transcription completes in the nucleus. We also observe that HIV-1 remains susceptible to a capsid destabilizing compound PF74 following nuclear import, revealing that uncoating completes in the nucleus. We also observe that certain CA mutants are insensitive to a Nup62 mediated nuclear pore blockade in cells which potently block infection by wild type CA, demonstrating that HIV-1 can utilize distinct nuclear import pathways during infection. These studies collectively define the spatiotemporal staging of critical steps of HIV-1 infection and provide an experimental system to separate and thereby define the cytoplasmic and nuclear stages of infection by other viruses.

Extensive examinations of the spatiotemporal staging of the HIV-1 lifecycle have supported a model in which HIV-1 completes reverse transcription and substantial capsid (CA)

*Corresponding Author: Edward M Campbell, 2160 South First Avenue, Maywood, IL, 60153, Phone: (708) 216-3345 ecampbell@luc.edu.

Author Contributions.

A.D and E.M.C designed the experiments. A.D, N.K, S.T and V.Z conducted the experiments. A.D, N.K, S.T and E.M.C analyzed the data. A.D and E.M.C wrote the manuscript. E.M.C supervised the study.

Supplementary Information is linked to the online version of the paper at www.nature.com/nature

Competing interests. The authors declare no competing financial interests. Correspondence and requests for materials should be addressed to E.M.C (ecampbell@luc.edu).

disassembly in the cytoplasm or at the nuclear pore complex[7,9,10]. The understanding of the spatiotemporal staging of these events has relied on both biochemical and imaging approaches. These studies have largely relied on monitoring indirect measures of nuclear import, such as the formation of 2-LTR circles[11] or the behavior of populations of viral particles that may or may not lead to productive infection.

To overcome these limitations and test this model of infection, we employed an inducible nuclear pore blockade (NPC) that allowed us to determine the spatiotemporal staging of reverse transcription, capsid disassembly and the kinetics of nuclear import of infectious HIV-1 viral particles following a synchronized infection. An inducible NPC blockade was achieved by transducing HIV-1 target cells with a lentiviral vector expressing Nup62 fused to a drug inducible dimerization domain (DmrB) and two copies of GFP (Fig 1a). Nup62 is a nucleoporin known to localize to the central pore of the NPC, and a previous study has demonstrated that a Nup62-DmrB-GFP (Nup62DG) fusion can allow for inducible ciliary and NPC blockade following addition of a rapamycin analog (HD) that induces homodimerization of the DmrB domain[12,13]. To monitor the efficacy of the Nup62DG construct to block active NPC transport, we monitored the nuclear translocation of estrogen receptor-α (ERα) induced by the addition of estradiol (E2). Consistent with previous observations, expression of this Nup62DG construct effectively prevented nuclear import of estrogen receptor-α (ERα) in the presence of the HD homodimerizing compound and E2 (Fig 1b, Extended Data Fig 1b). No difference in the rate of nuclear accumulation of ERα was observed following estradiol (E2) treatment was observed in the absence of HD treatment (Extended Data Figure 1a and 1c), demonstrating that Nup62DG expression does not perturb nuclear import when NPC blockade is not induced. Following infection with HIV-1 strain R7ΔEnvmCherry pseudotyped with VSV glycoproteins, cells stably expressing this construct was potently inhibited by addition of HD, while infection was not affected by expression of the construct or addition of HD alone (Fig 1c, Supplementary Figure 1). Nuclear pore blockade did not influence reverse transcription but did inhibit the formation of 2-LTR circles, a surrogate marker of nuclear import (Fig 1d), consistent with a specific block of HIV-1 nuclear import.

Visualization of HIV-1 particles in cells in which nuclear import was blocked revealed accumulation of HIV-1 particles at or near the nuclear membrane, often in complex with the Nup62DG construct (Fig 1e–f). In the absence of drug treatment, we also observed colocalization of HIV-1 with Nup62DG in the cytoplasm (Fig 1e). This was not specific to the Nup62DG construct, as we observed similar relocalization of endogenous Nup62 during infection and colocalization with HIV-1 following infection (Extended Data Fig 3), while Nup62 was almost exclusively localized to the NPC in the absence of infection. Live cell imaging revealed that HIV-1 trafficking in complex with Nup62DG away from the nuclear envelope following NPC blockade (Extended Data Fig 4, Supplementary video 1). These observations are similar to our previous observations of Nup358 relocalization during HIV-1 infection [14] and demonstrates that HIV-1 infection induces dynamic relocalization of numerous NPC components during infection.

We next utilized this selective nuclear pore blockade to determine HIV-1 nuclear import kinetics (NIK) in various target cells. Following a synchronized infection, nuclear pore

blockade was induced at various times following infection to determine the rate at which the viral inoculum became insensitive to nuclear pore blockade (Fig 2a). Notably, HIV-1 became resistant to nuclear pore blockade much quicker in monocytic and T cell lines, monocyte derived macrophages (MDMs) and CD4 positive primary T cells than HeLa cells (Fig 2), with approximately half of the inoculum becoming resistant to nuclear pore blockade ~3.5 hours following a synchronized infection in these cell types (Fig 2c–d), compared to ~7 hours in HeLa cells (Fig 2b).

The rate at which HIV-1 became insensitive to nuclear pore blockade suggested that HIV-1 nuclear import may occur prior to the completion of reverse transcription, which is generally considered to complete prior to nuclear import. Completion of reverse transcription occurs with much slower kinetics than the kinetics of nuclear import observed in cells, particularly in macrophages [15]. We therefore examined the rate at which HIV-1 became insensitive to nuclear pore blockade and RT inhibition in MDMs and THP-1 differentiated macrophages to test the hypothesis that nuclear import precedes completion of reverse transcription. These experiments revealed that the virus remains sensitive to RT inhibition for hours after the inoculum had become insensitive to the nuclear pore blockade (Fig 3a-b, Extended Data Fig 5). CD4+ T cells also remained sensitive to RT inhibition for hours after the viral inoculum became insensitive to NPC blockade (Fig 3c). Significant but less substantial differences noted in CEM and SupT1 T cell lines (Extended Data Fig 6a–b). Similar results obtained after infection with HIV-1 pseudotyped with CXCR4 tropic (HXB2) HIV-1 glycoproteins (Extended Data Fig 6c). Collectively, these data suggest that infectious HIV-1 virions enter the nucleus many hours before reverse transcription is complete. To validate this surprising observation, we ordered hybridization probes specific for each DNA strand formed during reverse transcription (Supplementary Figure 2). Consistent with the kinetics of nuclear import and reverse transcription sensitivity observed above, we observe that the puncta positive for both DNA strands did not appear until 9 hours PI and that these puncta were exclusively nuclear in THP-1 differentiated macrophages and MDMs (Fig 3d, Extended Data Fig 7a-b). These data collectively demonstrate that the viral ribonucleoprotein complex enters the nucleus prior to the completion of reverse transcription.

Prior studies have exhibited a lack of consensus regarding the role of reverse transcription in HIV-1 nuclear import. While some studies have shown that reverse transcription promotes cytoplasmic uncoating of the viral core prior to nuclear import [16–18], other studies have suggested that HIV-1 nuclear import can occur in the absence of reverse transcription [19]. To determine the degree to which cytoplasmic reverse transcription is required for functional nuclear import, we examined the nuclear import kinetics of cells infected in the presence of the RT inhibitor Nevirapine (NVP) for six hours. Although NVP treatment for 6 hours did not significantly impact infection measured at 48 hours in the absence of NPC blockade, we observed that the viral inoculum in the NVP treated infection remained unable to bypass the NPC blockade until NVP was washed out (Fig 3e–f, Extended Data Fig 8a). Following withdrawal of NVP, nuclear import of the inoculum rapidly recovered and approached the kinetics of nuclear import of untreated infections at later time points. Consistent with these observations, we also observe that NVP treatment prevented the relocalization of NPC components to the cytoplasm (Extended Data Fig 8b–f). However, we also observe that RT inhibition reduces but does not eliminate the accumulation of p24 CA in the nucleus

(Extended Data Fig 9a–b). These results collectively demonstrate that although reverse transcription can complete in the nucleus, some amount of cytoplasmic reverse transcription is necessary to facilitate productive nuclear import of the virus. The observation that reverse transcription is required to induce the relocalization of NPC components during infection is also consistent with a role for RT in HIV-1 nuclear import.

One reason that reverse transcription has generally been assumed to complete in the cytoplasm is that the strand transfer events which occur during reverse transcription likely require the constrained environment of the capsid core to prevent the premature diffusion of the reverse transcriptase enzyme away from the viral genome. However, most studies of core disassembly or uncoating suggest that this process completes prior to the nuclear import of the viral ribonucleoprotein complex (vRNPC)[1,20]. Although some CA protein has been shown to remain with the vRNPC in the nucleus[5–8], it has previously been difficult to demonstrate that this CA plays a functional role in infection subsequent to driving the final stages of nuclear import. We therefore used PF74, which is known to bind to the interface between CA monomers in assembled CA and inhibit infection[21–23]. PF74 susceptibility is therefore dependent on assembled CA and continued PF74 susceptibility after infection reveals a continued, functional role for assembled CA at subsequent steps of infection. We therefore used PF74 in the context of NIK assay to determine if assembled CA mediates a functional role in infection following nuclear import. As was observed with RT inhibitors, these experiments revealed that the viral inoculum remains sensitive to PF74 inhibition for hours after the virus becomes insensitive to nuclear pore blockade in all target cells examined (Fig 4). While this effect was more pronounced in MDMs, primary CD4+ T cells and THP-1 cells (Fig 4a–b, Fig 4e), we observed significant differences in nuclear pore blockade and PF74 sensitivity in SupT1 and CEM cells (Fig 4c–d), revealing that assembled CA mediates a functional step in infection subsequent to CA-mediated import of HIV-1.

Finally, as CA is known to mediate the nuclear import of HIV-1 and mutations in CA are reported to influence the nuclear import pathway utilized during infection [2,3], we next wanted to determine the degree to which CA mutants influence the nuclear import kinetics of HIV-1. However, infection with HIV-1 containing the N74D capsid, which is defective in binding to CPSF6 and Nup153 [3,4,24], and the P90A capsid, which cannot bind Cyclophilin A, exhibited substantially different susceptibility to NPC blockade as compared to WT virus in the same target cells (Extended Data Fig 10a–b). This suggests that these mutants, particularly the P90A mutant, enter the nucleus through distinct NPCs, consistent with a recently proposed model of NPC heterogeneity influencing HIV-1 infection and inhibition by the restriction factor MX2 [2].

In this study, we utilized an inducible NPC block to monitor the rate at which a synchronized HIV-1 infection becomes insensitive to NPC blockade. The ability to measure nuclear import under these conditions by monitoring HIV-1 infection provides substantial advantages over comparable imaging or biochemical approaches, thus allowing valuable insights into the spatiotemporal staging of key aspects of HIV-1 infection, including completion of reverse transcription and core disassembly. These results reveal that nuclear import occurs with faster kinetics than previously appreciated using 2-LTR circles to measure HIV-1 nuclear import. Nuclear import also precedes other events of the lifecycle,

including the completion of reverse transcription and uncoating, which have previously been considered to be cytoplasmic steps of HIV-1 infection. The observation that HIV-1 remains susceptible to PF74 following nuclear import reveals that assembled CA mediates a critical, nuclear step of infection which is independent of NPC translocation, as has been suggested by biochemical studies [21,25] and consistent with another study published online while this paper was in revision [26].

The relative insensitivity of the N74D and P90A CA mutants to Nup62-dimerization was another unexpected outcome in our study. While other studies support the notion that CA influences aspects of nuclear import and subsequent integration site selection[3,4,27], the selective blocking of individual CA mutants more specifically suggests that these viruses enter the nucleus through distinct nuclear pores which differ in their constituent nucleoporin composition. This possibility that nuclear pores are heterogeneous in nucleoporin composition and mediate import of different cargoes within individual cells is consistent with another recent study of HIV-1 nuclear import[2], but otherwise remains largely unappreciated and poorly characterized. Inducible dimerization of other NPC components may allow the composition of these alternative NPCs to be more clearly defined and allow the cytoplasmic and nuclear stages of HIV-1 infection, as well as infection of other viruses that enter the nucleus during infection, to be clearly established.

The observation that functional nuclear import (the nuclear import of infectious HIV-1) is inhibited when reverse transcription is inhibited is consistent with previous studies demonstrating that reverse transcription can induce HIV-1 uncoating in cells [16,17] and *in vitro* [28]. However, the observation that RT inhibition does not similarly reduce the amount of p24 in the nucleus (Fig 1f–g) is consistent with other studies suggesting that nuclear import of HIV-1 can occur independently of reverse transcription[7,26]. This observation, taken together with the observation that Nup62 blockade does not completely abolish infection (Fig 1c) and that some CA mutants can enter the nucleus using distinct nuclear import pathways (Extended Data Fig 10) suggest that differences in prior studies may be explained by the existence of multiple nuclear import pathways used by HIV-1. Our data suggests that reverse transcription promotes utilization of the primary import pathway utilized during infection, which our data suggests is more sensitive to Nup62 blockade than the alternative import pathways utilized by mutants such as P90A and N64D. The observation that p24 accumulation in the nucleus is not substantially reduced following inhibition of reverse transcription, but does not lead to infection, likely reflects the utilization of other nuclear import pathways not typically utilized during infection, such as those utilized by the P90A and N74D mutants. Consistent with this hypothesis, we have also observed that, similar to the case of RT inhibition (Extended Data Fig 8b–c), the N74D and P90A mutants do not induce the relocalization of NPC components during infection [14]. However, it is unclear why preventing the utilization of the predominant pathway by wt virus would not lead to productive infection in the context. Further characterization of the alternative nuclear import pathway or pathways HIV-1 can utilize during infection, and the development of similar tools to selectively block this pathway, should allow a better understanding of how utilization of distinct nuclear import pathways drives subsequent nuclear steps of infection of HIV-1.

Methods

Cell lines:

THP-1, CEM and SupT1 cells were obtained from ATCC. 293Ts and HeLa cells used in this study were cultured in Dulbecco's Modified Eagle Medium (DMEM) and THP-1, CEM and SuPT1 cells were cultured in RPMI medium (Cellgrow). Both media were supplemented with 10% characterized fetal bovine serum (FBS), 1000 U/ml penicillin, 1000 U/ml Streptomycin and 10 μg/ml Ciprofloxacin Hydrochloride. The cell lines used in this study were monitored for mycoplasma contamination by visualizing the DAPI stain. THP-1 cells were differentiated by treating the cells with 100 ng/ml phorbol myristate acetate (PMA, Sigma) for 48 h. Cells were cultured in normal media without PMA for another 24 h before performing experiments. To generate monocyte derived macrophages (MDM), peripheral blood mononuclear cells (PBMCs) were obtained from peripheral blood immediately after collection by layering over lymphocyte separation medium (Corning) and spinning at 400xg for 15 min. PBMCs were washed twice in PBS and monocytes were positively selected using the EasySep Human CD14 positive selection kit (STEMCELL) following the manufacturer's protocol. Isolated monocytes were resuspended in RPMI media supplemented with 10% fetal bovine serum (FBS), 1000 U/ml penicillin, 1000 U/ml Streptomycin and 10 μg /ml Ciprofloxacin Hydrochloride. Primary monocytes were differentiated into macrophages by resuspending in RPMI media containing 50 ng/ml granulocyte macrophage colony-stimulating factor (GM-CSF, R & D Systems) and 25 ng/ml macrophage colony-stimulating factor (M-CSF, R & D Systems). MDMs were differentiated for 10 days prior to experiments. To isolate primary CD4+ T cells from peripheral blood, PBMCs were isolated as described above and CD4+ cells were isolated using the EasySep Human CD4+ T cell Enrichment kit (STEMCELL) and were resuspended in RPMI media as above. Isolated CD4+ cells were stimulated with 2.5 μg/ml anti-CD3 (14–0037-82, Invitrogen), 2.5 μg/ml anti-CD28 (555726, BD Biosciences) and 10 ng/ml IL-2 (202-IL, R& D Systems) for 2 days prior to experiments.

Ethical Statement:

Human blood obtained in this study was from healthy anonymous donors (Loyola University IRB 208423) and informed consent was obtained from the participants.

Constructs:

The Nup62-DmrB-eGFP construct expressing mouse Nup62 was a kind gift from Dr. Kristen J Verhey, University of Michigan Medical School, Ann Arbor, Michigan. The mouse Nup62 in the above construct was replaced with the ORF from human Nup62 (Addgene Plasmid no 23559) and the resulting hNup62-DmrB-eGFP construct was recloned into the lentiviral backbone pLVX (Clontech). For expression of the above construct in primary CD4+ T cells and T cell lines, the hNUP62-DmrB-eGFP was cloned into the lentiviral backbone pAIP harboring the SFFV promoter, a gift from Jeremy Luban, University of Massachusetts Medical School (Addgene Plasmid no. 74171). The pLVX hNup62-DmrB-eGFP (plasmid # 139683) and pAIP hNup62-DmrB-eGFP (plasmid # 139684) are available through Addgene. Estrogen receptor alpha fused to mCherry was generated by cloning the estrogen receptor alpha ORF (Addgene Plasmid no 28230) into the pLVX-mCherry-

C1 backbone (Clontech). HIV-1 proviral plasmid R7ΔEnvmCherry was constructed by replacing the GFP component in the commonly used R7ΔEnvGFP reporter virus to mCherry.

Virus and vector production.

To generate HIV-1 particles pseudotyped with VSVg, 293T cells seeded in a 15cm dish at 70% confluency were transfected with 7 μg pCMV-VSVg and 18 μg of R7ΔEnvmCherry using polyethylenimine (PEI, MW 25000 Polysciences). To generate virus particles pseudotyped with HIV-1 envelope from HXB2 strain, 293T cells seeded in a 15cm dish at 70% confluency were transfected with 13 μg pCMV-HXB2g and 12 μg of R7ΔEnvmCherry using PEI. HIV-1 viruses harboring WT or mutant capsids were generated by transfecting 293Ts in 10cm dish with 3 μg p8.9NdsB (a gift from Jeremy Luban, University of Massachusetts Medical School) containing WT or the capsid mutations, 5 μg pLVX-mCherry and 2 μg pCMV-VSVg. Gag-Integrase-Ruby (GIR) labeled HIV-1 particles were generated by transfecting 293Ts in 10cm dish with 5 μg of R7ΔEnvmCherry, 3 μg of GIR and 2 μg of pCMV-VSVg. Vpx-containing VLPs were produced by the transfection of 293T cells in 15cm dish with 18 μg pSIV3^{+} and 7 μg of pCMV-VSVg. To generate viral vectors harboring the hNup62-DmrB-eGFP, 293Ts seeded on 15cm dish were transfected with 12 μg of either the pLVX-hNUp62-DmrB-eGFP or pAIP-hNUP62-DmrB-eGFP, 8 μg of packaging plasmid psPAX and 5 μg of pCMV-VSVg. Viruses were harvested 48 and 72 h post transfection and filtered through a 0.45 μm filter (Millipore). Viruses and viral vectors were concentrated by spinning at 4°C overnight at 5000xg. Synchronized infection of viruses and viral vectors on cells were performed by spinoculation at 13 °C for 2 h at 1200xg.

Generation of stable cell lines and transduction of primary macrophages and CD4+ T cells:

To generate HeLa and THP-1 cell lines stably expressing the hNup62-DMRB-eGFP, viral vectors produced using the pLVX-hNup62-DmrB-eGFP construct were used for transduction. To select for the stably transduced population, cells were treated with 2 μg/ml puromycin (Gibco) 48 h following transduction. Viral vectors produced from pAIP-hNUP62-DmrB-eGFP were used to transduce CEM and SupT1 cells. For these cells, selection was carried out using 1 μg/ml puromycin.

To transduce monocyte derived macrophages (MDM) with the pLVX-hNUP62-DmrB-eGFP, primary monocytes undergoing differentiation to macrophages were treated overnight with SIV Vpx VLPs on Day 5 and on Day 6 then the cells were synchronously infected with a concentrated stock of Nup62 vector. On Day 7, vector containing media was replaced with normal media containing GM-CSF and M-CSF. On day 10 (4 days following transduction), MDM expressing the hNUP62-DmrB-eGFP construct were synchronously infected with concentrated stock of HIV-1 strain R7ΔEnvmCherry pseudotyped with VSV glycoproteins, and the NIK assay was performed. Infectivity was measured 96 h following synchronized infection.

To transduce CD4+ T cells, cells were stimulated for 2 days with anti-CD3/CD28 and IL-2 then were transduced with a concentrated stock of pAIP-hNUP62-DmrB-eGFP and spinoculated at 800xg for 1 h at 32°C. Vector containing media was changed 24 hours later.

4 days following transduction, CD4+ T cells expressing the hNup62-DmrB-GFP construct were synchronously infected with concentrated stock of HIV-1 strain R7ΔEnvmCherry pseudotyped with VSV glycoprotein, and the NIK assay was performed as described below. Infectivity was measured 48 h post synchronized infection.

HIV-1 Nuclear Import Kinetics (NIK) Assay:

TheNIK assay was performed as outlined in Fig 2a.Cells stably expressing or transduced with the hNUP62-DmrB-eGFP construct were plated in 48 well plates. Dividing cells were pretreated overnight with 10 μg/ml of Aphidicolin to arrest cell division and ensure viral entry through the nuclear pore complex. Cells were synchronously infected with HIV-1 strain R7ΔEnvmCherry pseudotyped with VSVg or HIV-1 Env glycoproteins by spinoculation at 13°C for 2 h at 1200xg. Following spinoculation, media was replaced with warmed 37°C normal media. Homodimerizing drug (HD) at a final concentration of 1.5 μM was added to block active nuclear pore transport immediately after the synchronized infection (time point 0 h) or added at the indicated time post-infection as depicted in Fig 2a. 24 h post synchronized infection, HD containing media was removed, cells were washed and cultured in normal media. Infectivity was measured 48 h post synchronized infection for all cells expect MDMs, in which case infectivity was measured 96 h post infection. Infectivity determined by measuring the percentage of mCherry positive cells using the BD LSRFortessa flow cytometer (BD Bioscience). The percentage of mCherry positive cells was calculated as the ratio of the double positive population (Nup62eGFP+, R7mCherry+) over the total amount of Nup62GFP+ population (Extended Data Fig 2b).

Antibodies and Chemicals:

HIV-1 capsid protein, p24, was stained using either anti-p24 183-H12–5C (HIV-1 p24 hybridoma from Dr. Bruce Chesebro) and obtained through the NIH AIDS Reagent Program, Division of AIDS, NIAID, NIH or using HIV-1 p24 antibody (24–4) from Santa Cruz Biotechnology, INC (sc-69728). Rabbit polyclonal antibody against Lamin A/C (10298–1-AP) and Nup62 (13916–1-AP) used for immunofluorescence experiments were purchased from Proteintech. Rabbit polyclonal antibody against Nup358 (ab64276) was purchased from Abcam. Mouse monoclonal antibody against Nup62 (sc-48389) and GAPDH (sc-47724) used for western blotting were purchased from Santa Cruz Biotechnology, INC. Secondary antibodies conjugated to a fluorophore were used for immunofluorescence studies and were purchased from Jackson Immunoresearch Laboratories. B/B Homodimerizer (HD drug) was purchased from Clontech (635059). PF74, Nevirapine (NVP), estradiol and DAPI stain were obtained from Sigma Aldrich. Aphidicolin was purchased from Cayman Chemicals.

Western Blotting:

Cell lysates were prepared by lysing cells with NP-40 lysis buffer (100mM Tris pH 8.0, 1% NP-40, 150 mM NaCl) containing protease inhibitor cocktail (Roche) for 10 minutes on ice. Following incubation, lysates were spun down at 13,000 rpm for 10 min and supernatant was collected for western blot analysis. In brief, 2x Laemmli sample buffer was added to the lysed sample and incubated at 100°C for 5 min. Protein concentration was measured using Pierce BCA protein assay kit (Thermo Scientific) and equal amounts of

protein were loaded onto a 4–15% gradient gel (Bio-Rad). Upon separation, the proteins were transferred to nitrocellulose membranes (Bio-Rad). Membranes were incubated with specific primary antibodies overnight and then incubated with secondary antibodies conjugated to horseradish peroxidase (HRP) (Thermo Scientific). Antibody complexes were detected using SuperSignal™ West Femto Chemiluminescent Substrate (Thermo Scientific). Chemiluminescence was detected using the FluroChem Imaging system (ProteinSimple).

Microscopy and Image acquisition:

Z-stack images were collected with a DeltaVision wide field fluorescence microscope (Applied Precision, GE) equipped with a digital camera (CoolSNAP HQ; Photometrics) and a 1.4-numerical aperture 100× objective lens. Excitation light was generated with an Insight SSI solid state illumination module (Applied Precision, GE), and the images were deconvolved with SoftWoRx deconvolution software (Applied Precision, GE). In all experiments, identical acquisition conditions were used to acquire all images. Following deconvolution, images were analyzed using Imaris 8.4.1 (Bitplane). An algorithm was designed using the surface function in Imaris to generate surfaces around the signal of interest and the maximum fluorescence intensity detected within these surfaces was measured. The same algorithm was applied to all images within an experiment. For live cell experiments, cells were plated on delta DPG dishes (Thermo Fisher Scientific) and maintained at 5% CO_2 and 37 °C in an environmental chamber on a DeltaVision microscope.

Quantitative PCR:

Cells were infected with equal MOI and RT-PCR was performed to determine the relative expression of the late reverse transcription (Late RT) and 2-LTR products. The following primers targeting the HIV-1 Pol were used to quantify Late RT, Pol Fwd, 5’-GGGAGCCACACAATGAATG-3’ and Pol rev, 5’-CCAGGGCTCTAGTCTAGGATC-3’. The 2-LTR primers used were described previously[29]. GAPDH was used as the housekeeping gene for normalization. In brief, genomic DNA from cells was extracted following the DNeasy Blood and Tissue Kit protocol (Qiagen). DNA concentration was determined and equal amounts of DNA were digested with Dpn1 (New England BioLabs) before performing RT-PCR.

In Situ vDNA detection:

To detect negative and positive HIV-1 vDNA strands, probes targeting the antisense strand (detects negative vDNA) or the sense strand (detects positive vDNA) and the detection reagents were purchased from Advanced Cell Diagnostics (ACD). Negative vDNA was detected using the ACD probe HIV-gagpol-sense (317701) and positive vDNA was detected using the ACD probe HIV-C2 (446211-C2). The assay was performed according to the manufacturer’s protocol and as previously described[30]. In brief, following fixation with 3.7% paraformaldehyde (PFA), cells on coverslips were dehydrated with the sequential addition of 50%, 70% and 100% ethanol for 5 min each at room temperature. To rehydrate cells, the sequential addition of ethanol was reversed and cells were incubated with each solution for 2 min at room temperature. Following rehydration, cells were treated with protease solution (Pretreat 3) diluted in PBS (1:2 dilution) for 15 min in a humidified

HybEZ (ACD) oven at 40°C. Following protease treatment, samples were washed three times with molecular grade water and then treated with 5 mg/ml RNase A (Qiagen) in PBS for 30 min at 37°C. Cells were then washed three times with molecular grade water and heated at 55°C for 30 min with hybridization buffer as described[30]. The hybridization buffer was removed and probes were diluted in hybridization buffer (1:1 for Negative vDNA C1 probe and 1:50 for Positive vDNA C2 probe) and allowed to hybridize with samples in the humidified HybEZ oven at 40°C for 2 h. Following hybridization with the samples, the probes were visualized by hybridizing with preamplifiers, amplifiers and a fluorescent label as per the manufacturer's protocol for probe detection (RNAscope Multiplex Fluorescent Detection Kit, ACD).

Proximity Ligation Assay:

Duolink proximity ligation assay (PLA) kitwas purchased from Sigma, and the assay was performed as previously described[14]. In brief, cells were grown on coverslips and fixed with 3.7% PFA. To detect the interaction between viral capsid protein, p24, and Nup358, cells were permeabilized and blocked in 3% BSA followed by incubation with primary antibodies targeting viral protein p24 (mouse monoclonal) and Nup358 (rabbit polyclonal). After primary staining, coverslips containing cells were washed and incubated (1h, 37°C) with secondary anti-mouse conjugated with minus and anti-rabbit conjugated with plus Duolink II PLA probes. Coverslips were washed again and incubated with ligation-ligase solution (30min, 37°C) followed by washing and subsequent incubation with amplification-polymerase solution (100min, 37°C) containing Duolink II in situ detection reagent Red. Finally, coverslips were washed and mounted with Duolink II mounting media containing DAPI. Interactions were detected as fluorescent spots ($\lambda_{\text{excitation/emission}}$ 598/634 nm) with a fluorescence microscope.

Quantification of perinuclear and cytoplasmic protein signal:

Quantification of p24, Nup358 or Nup62 signal in the cell was performed following the similar quantification method described in our previous study [14].Nuclear and perinuclear signal was determined using surface masks around the nucleus created based on the DAPI channel. To detect perinuclear and nuclear signal, an algorithm was created which reliably overestimates the size of the nucleus, as previously described [14] (Extended Data Fig 3a). The perinuclear algorithm to detect cell nuclei included all z sections acquired. All events within this mask were considered nuclear and perinuclear, while all events outside of this mask were considered cytoplasmic, as determined using the surface function and masking tool in Imaris 8.4.1.

To detect nuclear signal, an algorithm was designed to detect the cell nuclei using the DAPI channel as reference and surface function in Imaris 8.4.1 (Extended Data Fig 3b). z sections close to the top or bottom of the nucleus were excluded to avoid detection of extranuclear signal. Similar to above, all events within the mask were considered nuclear and all events outside the mask were considered perinuclear and cytoplasmic. The amount of perinuclear signal was quantified by subtracting the signal obtained from nuclear and perinuclear signal to signal obtained from nuclear signal.

Statistical Analysis:

GraphPad Prism version 6.00 (GraphPad Software, Inc.) was employed for statistical analysis and to make graphs. Statistical significance was assessed using the Two-way ANOVA and Bonferroni post test. $P<0.05$ was considered significant in our experiments. Data were represented as mean +/− SEM depending on the graph. All 446 statistics for NIK assays are provided as source data.

Data availability statement.

The Nup62-DmrB-GFP plasmids used in this study are deposited to Addgene and relevant information provided in the methods section. All data generated or analyzed during this study are presented in the paper or in the supplementary information or as source data. All data are available from the corresponding author upon reasonable request.

Extended Data

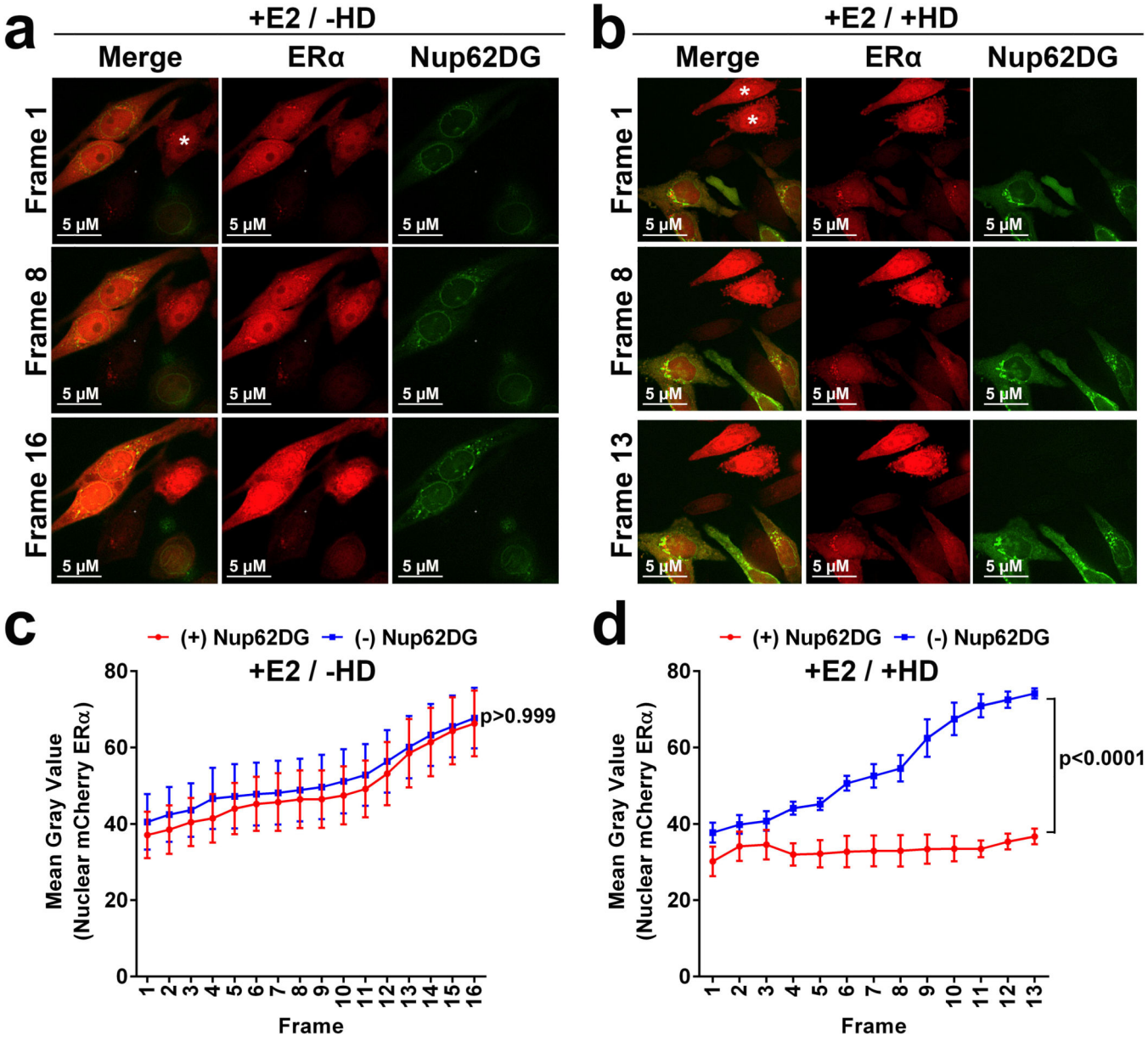

Extended Data Fig. 1. Expression of the Nup62 dimerization construct in cells does not alter normal cell physiology

a, HeLa cells were transduced simultaneously with lentiviral vectors driving expression of Nup62DG or mCherry-estrogen receptor alpha (ERα). Imaging fields were selected that contain cells expressing only ERα (marked by asterisk) or both ERα and Nup62DG. Live cell imaging was performed after addition of estradiol (E2) to mediate nuclear translocation of ERα. Images acquired every four minutes for a total of one hour. **b,** Similar experiment as in (a) except the cells were treated with the homodimerizing drug (HD) to block NPC transport along with E2 treatment. **c**, Accumulation of mCherry-ERα fluorescence in the nuclear region was monitored in Nup62DG+ and Nup62DG- cells treated with E2 using

ImageJ plugin Time Series Analyzer V3. Depicted mean values from three independent experiments (±SEM). **d,** similar quantification as in (c) in cells treated with E2 and HD. Error bar represents SEM. Statistical significance was assessed using Two-way ANOVA and Bonferroni post test. P<0.05 was considered significant in our experiments.

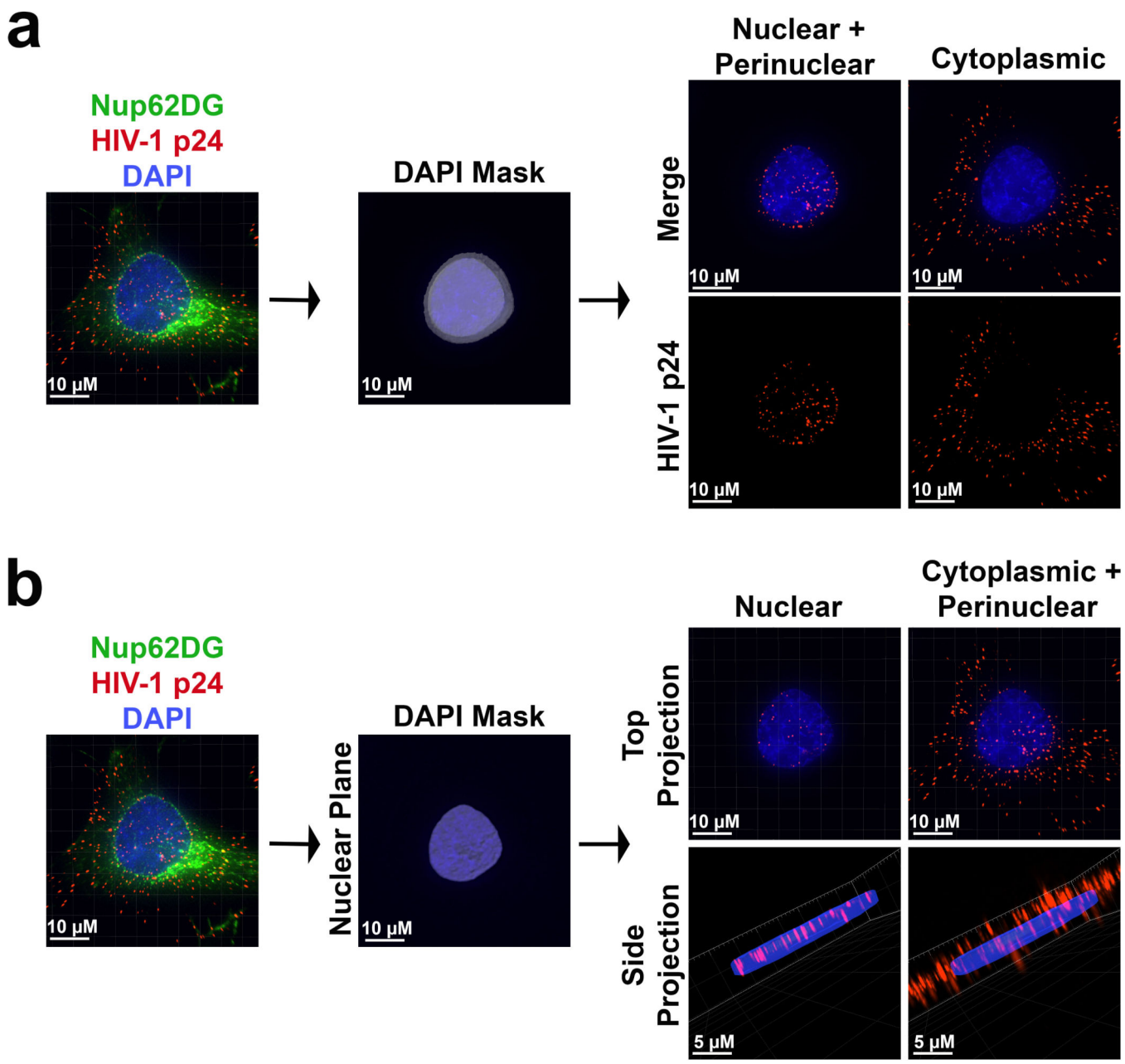

Extended Data Fig. 2. Quantification strategy employed to quantify nuclear, perinuclear and cytoplasmic signal using Imaris

Schematic representation of the quantification technique used in this manuscript with an example image of a cell expressing the Nup62DG and infected with HIV-1. Cells were stained for the capsid protein p24 and DAPI. **a,** Nuclear and perinuclear signal was quantified using a DAPI mask generated using the surface function in Imaris that exceeded

the boundary of DAPI stain to include the perinuclear signal. As depicted, all signal within this mask was considered nuclear and perinuclear signal. Similarly, all signal outside of this mask was considered cytoplasmic signal. **b,** To focus on exclusively nuclear signal, an algorithm which reliably identified the nuclear boundary, as indicated by a DAPI stain, was generated in Imaris. Sections close to the upper and lower boundary of the nucleus (in Z) were removed to focus analysis on nuclear events. As in (a) signal within this mask was considered nuclear and all signal outside this mask was considered cytoplasmic and perinuclear.

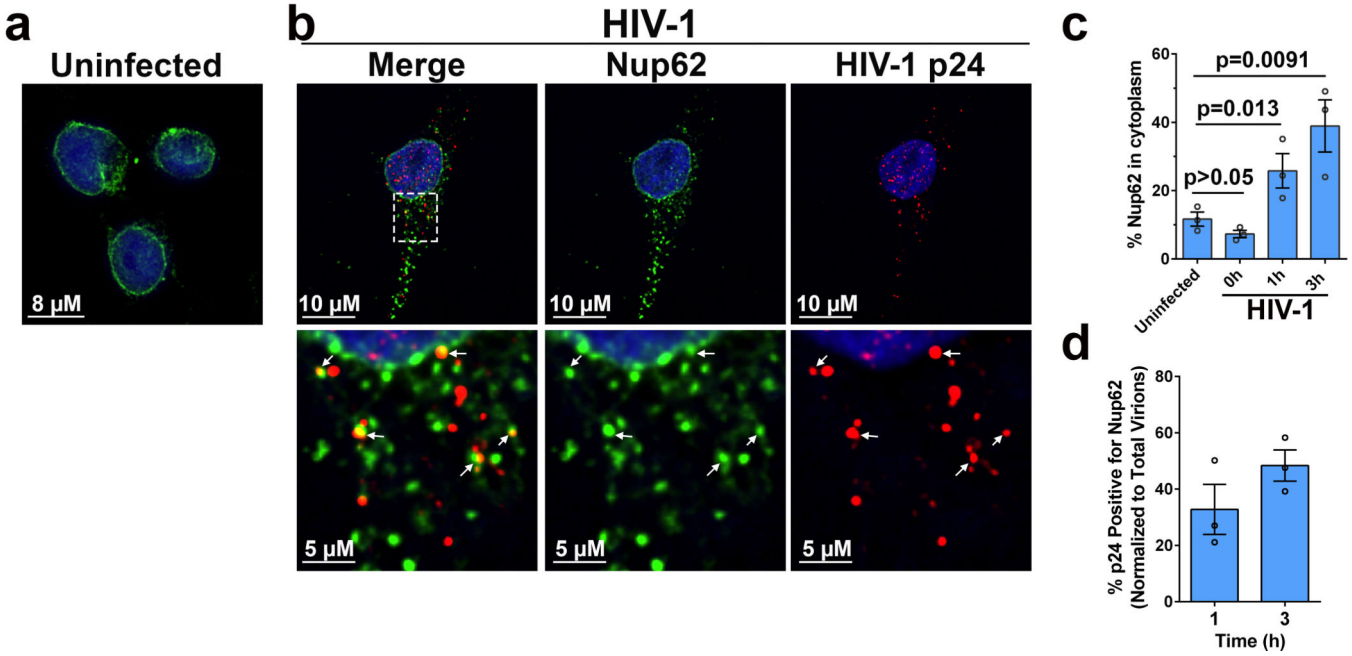

Extended Data Fig. 3. HIV-1 infection induces Nup62 relocalization and colocalization with HIV-1 cores in the cytoplasm

a, Nup62 localization in uninfected HeLa cells. **b**, HeLa cells synchronously infected with VSVg-R7ΔEnvmCherry at 3 h post infection, fixed and stained for Nup62 (green), HIV-1 capsid protein p24 (red), and DAPI (blue) for cell nuclei. Enlarged view of colocalization (boxed region) between Nup62 and HIV-1 capsid protein p24 shown in the bottom panel and indicated by arrows. **c**, Quantification of cytoplasmic Nup62, as described in methods section and supplementary Fig 2a. 20 or more cells analyzed per sample. Data averaged from three independent experiments. Error bar represents SEM. **d**, Quantification of the percent p24 colocalizing with Nup62 in HeLa cells. 20 or more cells analyzed per sample. Data averaged from three independent experiments. Error bar represents SEM. Statistical significance was assessed using Two-way ANOVA and Bonferroni post test. $P<0.05$ was considered significant in our experiments.

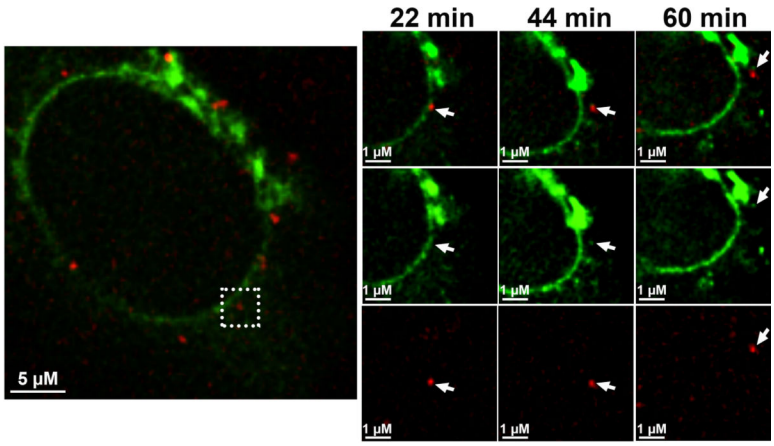

Extended Data Fig. 4. HIV-1 particles retained at the NPC over extended period upon Nup62 dimerization.

HeLa cells expressing Nup62DG synchronously infected with Gag-Integrase-Ruby (GIR) labeled HIV-1 particles. 1 hour following synchronized infection, cells were treated with homodimerizing drug (HD) and imaged every 4 minutes for 1 hour. Snapshot of a GIR labeled virus particle (boxed region) at the indicated times during acquisition is shown. Similar pattern observed across 5 independent experiments.

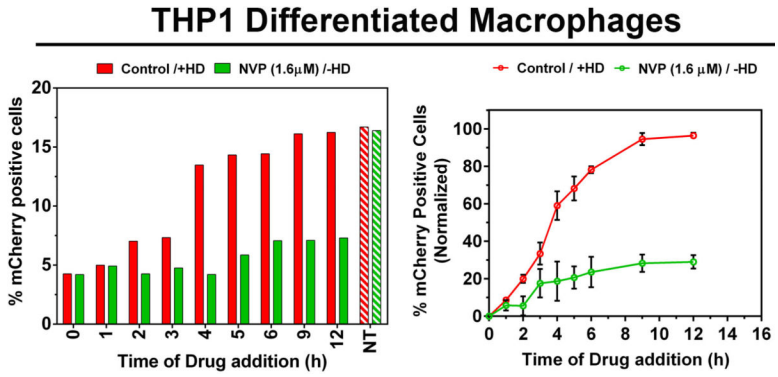

Extended Data Fig. 5. Monitoring reverse transcription with a low dose of RT inhibitor nevirapine to mirror the level of inhibition induced by Nup62DG blockade

THP1 cells expressing the Nup62DG were differentiated to macrophages and infected with VSVg- R7ΔEnvmCherry and NIK monitored by HD addition (red) as described in Fig 2. To monitor replication kinetics, cells incubated with HIV-1 reverse transcriptase inhibitor Nevirapine (NVP, 1.6 μM) at different time's post infection as depicted (green) and washed off at 24 h. Infection measured as described in Fig 2. Bar graphs depict data from a single experiment and line graphs depict normalized and average data (±SEM) as described in Fig 2 from three independent experiments. NT represents no treatment.

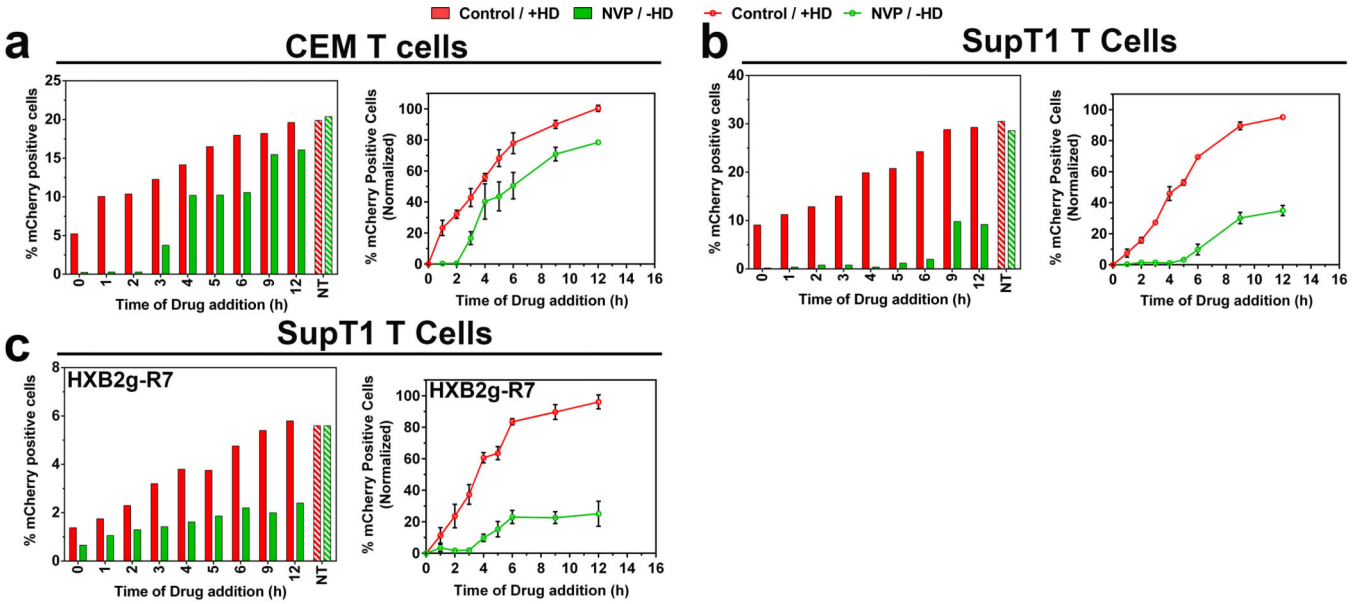

Extended Data Fig. 6. HIV-1 reverse transcription completes in the nucleus of infected T cells

a-b, CEM and SupT1 expressing the Nup62DG infected with VSVg- R7ΔEnvmCherry and NIK monitored by HD addition (red) as described in Fig 2. To monitor replication kinetics, cells incubated with HIV-1 reverse transcriptase inhibitor Nevirapine (NVP, 5μM) at different time's post infection as depicted (green) and washed off at 24 h. Infection measured as described in Fig 2. **c,** Similar experiment as above done on SupT1 cells expressing Nup62DG after infection with R7ΔEnvmCherry pseudotyped with HIV-1 envelope from the HXB2 strain. All bar graphs depict data from a single experiment and line graphs depict normalized and average data (±SEM) as described in Fig 2 from three independent experiments. NT represents no treatment.

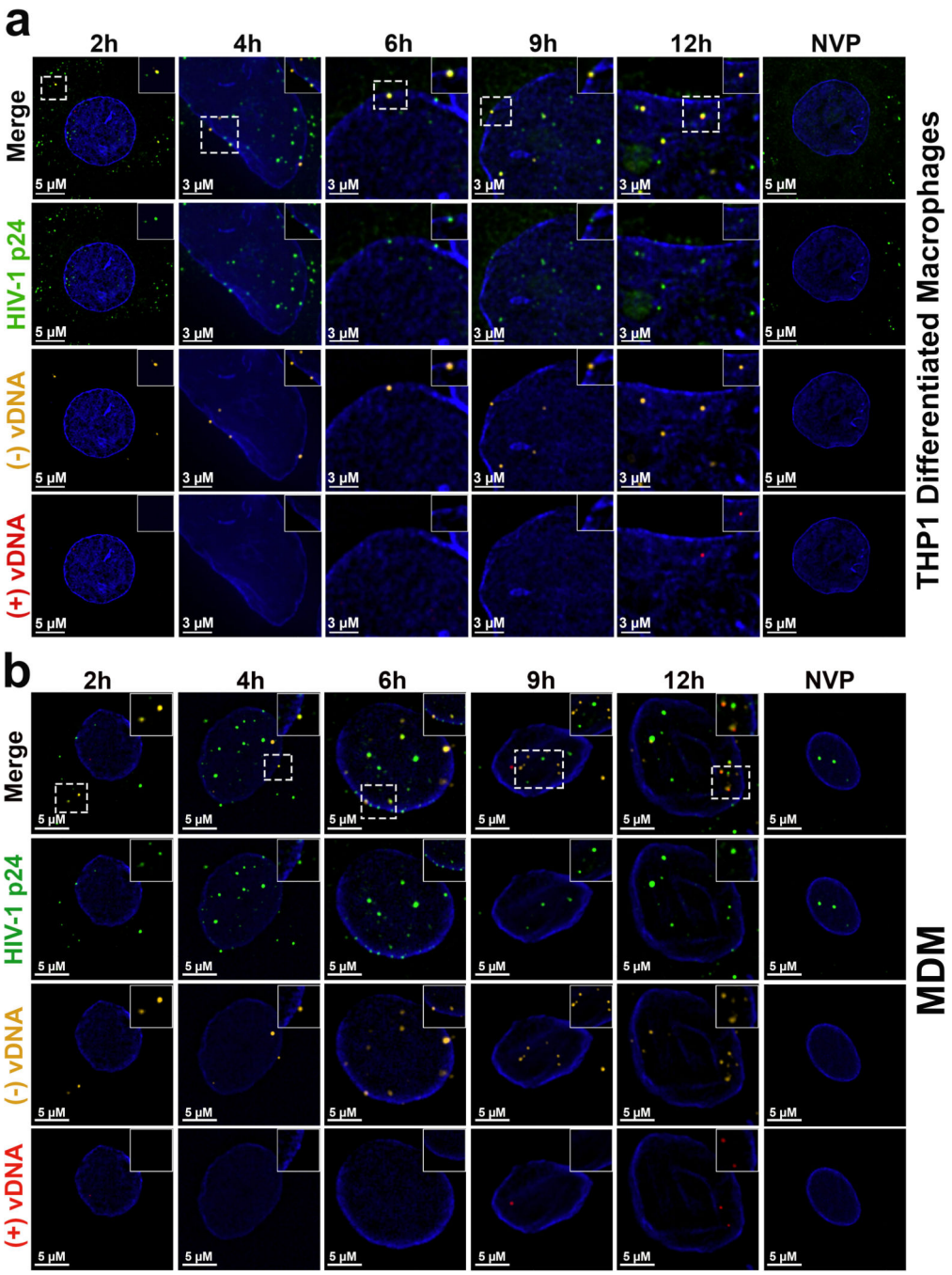

Extended Data Fig. 7. Positive strand HIV1 vDNA colocalize with Negative strand only in the nucleus of infected THP1 differentiated macrophages and primary macrophages

a,b. THP1 differentiated macrophages (a) and monocyte derived macrophages (b) synchronously infected with VSVg- R7ΔEnvmCherry and fixed at different times post synchronized infection. Cells treated with RNase A and stained for (–) VDNA (orange) and (+) vDNA (red) using specific sense and antisense probes. Upon probe staining, these cells were also stained for HIV-1 capsid protein p24 (green) and nuclear Lamin A/C (blue). Depicted a representative image at the indicated time points. Data shown here is representative of three independent experiments. Quantification provided in Fig 3d.

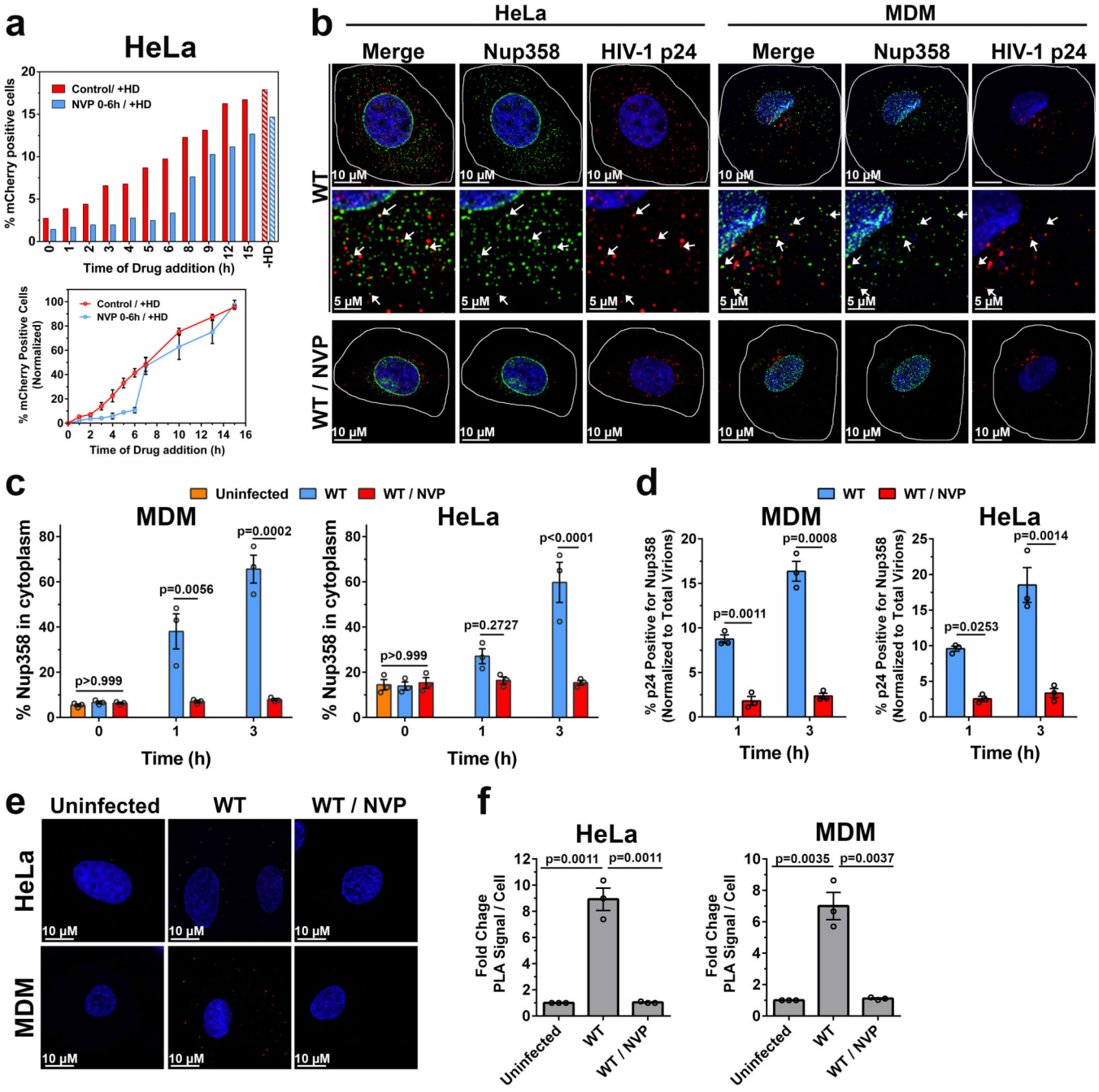

Extended Data Fig. 8. Nup358 relocalization induced upon HIV-1 infection absent upon inhibition of HIV-1 reverse transcription

a, HeLa cells expressing the Nup62DG infected with VSVg- R7ΔEnvmCherry and NIK monitored by HD addition alone (red) or in the presence of NVP treatment for the first 6 hours (blue) following synchronized infection. Bar graphs depict data from a single experiment and line graphs depict normalized and average data (±SEM) as described in Figure 2 from three independent experiments. **b**, HeLa cells and primary human macrophages (MDM) synchronously infected with HIV-1 (WT) and treated with HIV-1 reverse transcriptase inhibitor NVP. Cells fixed 0, 1 and 3 h (shown) post infection and

stained for Nup358 (green), HIV-1 capsid protein p24 (red), and DAPI (blue). Middle panel depicts colocalization between Nup358 and p24. Data shown here is representative of three independent experiments. **c,d,** Percent Nup358 in the cytoplasm and percent p24 colocalizing with Nup358 at the different times post infection in HeLa and MDM. 20 or more cells analyzed in each experiment. Data averaged (mean) from three independent experiment. **e,** Proximity ligation assay performed in HeLa and MDM after HIV-1 infection and cells fixed 3h post infection. Each red puncta represents a positive PLA signal generated by interaction of Nup358 and p24. **f,** Average fold increase in PLA signal, relative to uninfected control, from three independent experiments. 20 or more cells analyzed in each experiment. Error bar represents SEM. All statistical significance was assessed using Two-way ANOVA and Bonferroni post test. P<0.05 was considered significant in our experiments.

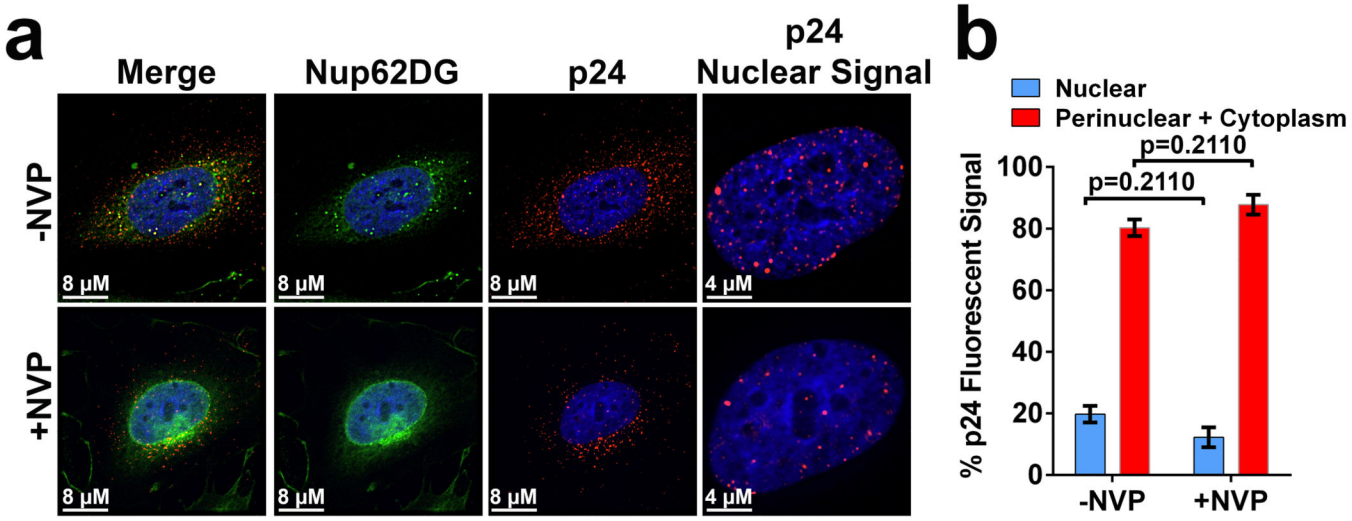

Extended Data Fig. 9. Nuclear p24 signal upon inhibition of reverse transcription

a, HeLa cells expressing Nup62DG infected with VSVg- R7ΔEnvmCherry and treated with HIV-1 reverse transcriptase inhibitor NVP for 7 hours following synchronized infection. Cells fixed and stained for HIV-1 capsid protein p24 (red), and DAPI (blue). **b,** Quantification of nuclear HIV-1 p24 signal, performed as described in methods and supplementary Fig 2b. 20 or more cells analyzed in each experiment. Data averaged from three independent experiments. Error bar represents SEM. Statistical significance was assessed using Two-way ANOVA and Bonferroni post test. P<0.05 was considered significant in our experiments.

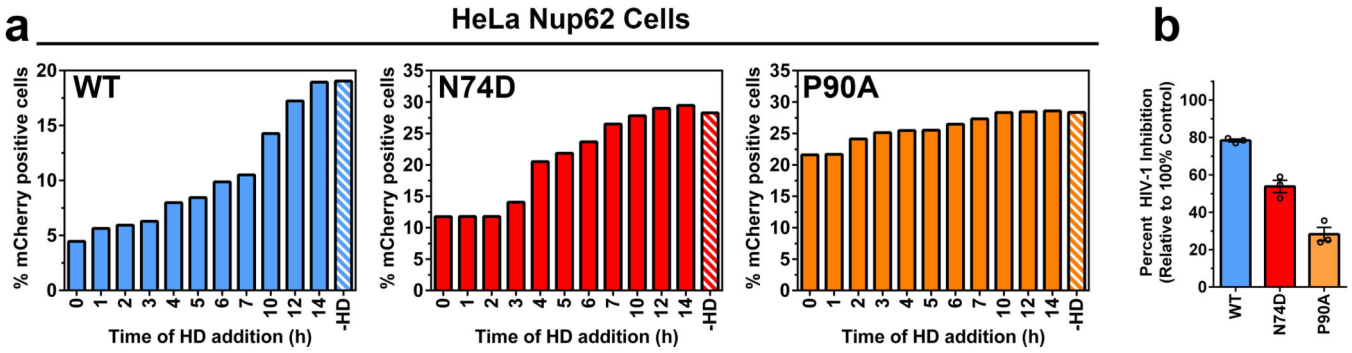

Extended Data Fig. 10. Insensitivity of the capsid mutants N74D and P90A to the Nup62 mediated artificial nuclear pore block suggests heterogeneity in the nuclear pores and usage by WT virus

HeLa cells stably expressing the Nup62DG infected with HIV-1 harboring either the WT capsid (blue) or capsid mutants N74D (red) and P90A (orange). NIK measured in these cells by HD addition as described in Fig 2. **a**, Shown a bar graph from a single experiment. **b**, Percent inhibition attained upon blocking the nuclear pore for the first 24 h. Data averaged from three independent experiments. Error bar represents SEM.

Supplementary Material

Refer to Web version on PubMed Central for supplementary material.

Acknowledgements.

We thank Dr. Kristen Verhey for kindly providing us with constructs required for the study. We are grateful to anonymous blood donors who contributed leukocytes to this study. The authors would like to thank Stephanie Zack for proof reading the article. This work was supported by NIH grant R21AI139009 to E.M.C.

References:

1. Campbell EM & Hope TJ HIV-1 capsid: the multifaceted key player in HIV-1 infection. Nat Rev Microbiol13, 471–483, doi:10.1038/nrmicro3503nrmicro3503 [pii] (2015). [PubMed: 26179359]
2. Kane M et al. Nuclear pore heterogeneity influences HIV-1 infection and the antiviral activity of MX2. Elife7, doi:10.7554/eLife.35738 (2018).
3. Lee K et al. Flexible use of nuclear import pathways by HIV-1. Cell Host Microbe7, 221–233, doi:10.1016/j.chom.2010.02.007S1931-3128(10)00070-3 [pii] (2010). [PubMed: 20227665]
4. Schaller T et al. HIV-1 capsid-cyclophilin interactions determine nuclear import pathway, integration targeting and replication efficiency. PLoS Pathog7, e1002439, doi:10.1371/journal.ppat.1002439PPATHOGENS-D-11-01130 [pii] (2011).
5. Bejarano DA et al. HIV-1 nuclear import in macrophages is regulated by CPSF6-capsid interactions at the nuclear pore complex. Elife8, doi:10.7554/eLife.41800 (2019).
6. Chin CR et al. Direct Visualization of HIV-1 Replication Intermediates Shows that Capsid and CPSF6 Modulate HIV-1 Intra-nuclear Invasion and Integration. Cell Rep13, 1717–1731, doi:10.1016/j.celrep.2015.10.036S2211-1247(15)01206-1 [pii] (2015). [PubMed: 26586435]
7. Francis AC & Melikyan GB Single HIV-1 Imaging Reveals Progression of Infection through CA-Dependent Steps of Docking at the Nuclear Pore, Uncoating, and Nuclear Transport. Cell Host Microbe23, 536–548 e536, doi:10.1016/j.chom.2018.03.009 (2018). [PubMed: 29649444]
8. Hulme AE, Kelley Z, Foley D & Hope TJ Complementary Assays Reveal a Low Level of CA Associated with Viral Complexes in the Nuclei of HIV-1-Infected Cells. Journal of virology89, 5350–5361, doi:10.1128/JVI.00476-15 (2015). [PubMed: 25741002]

9. Hu WS & Hughes SH HIV-1 reverse transcription. Cold Spring Harb Perspect Med 2, doi:10.1101/cshperspect.a006882 (2012).
10. Mamede JI, Cianci GC, Anderson MR & Hope TJ Early cytoplasmic uncoating is associated with infectivity of HIV-1. Proc Natl Acad Sci U S A114, E7169–E7178, doi:10.1073/pnas.1706245114 (2017). [PubMed: 28784755]
11. Butler SL, Hansen MS & Bushman FD A quantitative assay for HIV DNA integration in vivo. Nat Med7, 631–634 (2001). [PubMed: 11329067]
12. Takao D et al. An assay for clogging the ciliary pore complex distinguishes mechanisms of cytosolic and membrane protein entry. Current biology : CB24, 2288–2294, doi:10.1016/j.cub.2014.08.012 (2014). [PubMed: 25264252]
13. Clackson T et al. Redesigning an FKBP-ligand interface to generate chemical dimerizers with novel specificity. Proc Natl Acad Sci U S A95, 10437–10442, doi:10.1073/pnas.95.18.10437 (1998). [PubMed: 9724721]
14. Dharan A et al. KIF5B and Nup358 Cooperatively Mediate the Nuclear Import of HIV-1 during Infection. PLoS Pathog12, e1005700, doi:10.1371/journal.ppat.1005700 (2016).
15. Bejarano DA et al. Detailed Characterization of Early HIV-1 Replication Dynamics in Primary Human Macrophages. Viruses10, doi:10.3390/v10110620 (2018).
16. Cosnefroy O, Murray PJ & Bishop KN HIV-1 capsid uncoating initiates after the first strand transfer of reverse transcription. Retrovirology13, 58, doi:10.1186/s12977-016-0292-7 (2016). [PubMed: 27549239]
17. Hulme AE, Perez O & Hope TJ Complementary assays reveal a relationship between HIV-1 uncoating and reverse transcription. Proc Natl Acad Sci U S A108, 9975–9980, doi:1014522108 [pii] 10.1073/pnas.1014522108 (2011). [PubMed: 21628558]
18. Yang Y, Fricke T & Diaz-Griffero F Inhibition of reverse transcriptase activity increases stability of the HIV-1 core. J Virol 87, 683–687, doi:10.1128/JVI.01228-12JVI.01228-12 [pii] (2013). [PubMed: 23077298]
19. Burdick RC et al. Dynamics and regulation of nuclear import and nuclear movements of HIV-1 complexes. PLoS Pathog13, e1006570, doi:10.1371/journal.ppat.1006570 (2017).
20. Wu X, Anderson JL, Campbell EM, Joseph AM & Hope TJ Proteasome inhibitors uncouple rhesus TRIM5alpha restriction of HIV-1 reverse transcription and infection. Proc Natl Acad Sci U S A103, 7465–7470 (2006). [PubMed: 16648264]
21. Balasubramaniam M et al. PF74 Inhibits HIV-1 Integration by Altering the Composition of the Preintegration Complex. J Virol 93, doi:10.1128/JVI.01741-18 (2019).
22. Bhattacharya A et al. Structural basis of HIV-1 capsid recognition by PF74 and CPSF6. Proc Natl Acad Sci U S A111, 18625–18630, doi:10.1073/pnas.1419451121419945112 [pii] (2014). [PubMed: 25518861]
23. Saito A et al. Roles of Capsid-Interacting Host Factors in Multimodal Inhibition of HIV-1 by PF74. J Virol90, 5808–5823, doi:10.1128/JVI.03116-15 (2016). [PubMed: 27076642]
24. Matreyek KA & Engelman A The requirement for nucleoporin NUP153 during human immunodeficiency virus type 1 infection is determined by the viral capsid. J Virol85, 7818–7827, doi:10.1128/JVI.00325-11JVI.00325-11 [pii] (2011). [PubMed: 21593146]
25. Chen NY et al. HIV-1 capsid is involved in post-nuclear entry steps. Retrovirology13, 28, doi:10.1186/s12977-016-0262-0 (2016). [PubMed: 27107820]
26. Burdick RC et al. HIV-1 uncoats in the nucleus near sites of integration. Proc Natl Acad Sci U S A, doi:10.1073/pnas.1920631117 (2020).
27. Achuthan V et al. Capsid-CPSF6 Interaction Licenses Nuclear HIV-1 Trafficking to Sites of Viral DNA Integration. Cell Host Microbe24, 392–404 e398, doi:10.1016/j.chom.2018.08.002 (2018). [PubMed: 30173955]
28. Rankovic S, Ramalho R, Aiken C & Rousso I PF74 Reinforces the HIV-1 Capsid To Impair Reverse Transcription-Induced Uncoating. J Virol92, doi:10.1128/JVI.00845-18 (2018).
29. Anderson JL et al. Proteasome inhibition reveals that a functional preintegration complex intermediate can be generated during restriction by diverse TRIM5 proteins. J Virol80, 97549760 (2006).

30. Puray-Chavez M et al. Multiplex single-cell visualization of nucleic acids and protein during HIV infection. Nat Commun8, 1882, doi:10.1038/s41467-017-01693-z (2017). [PubMed: 29192235]

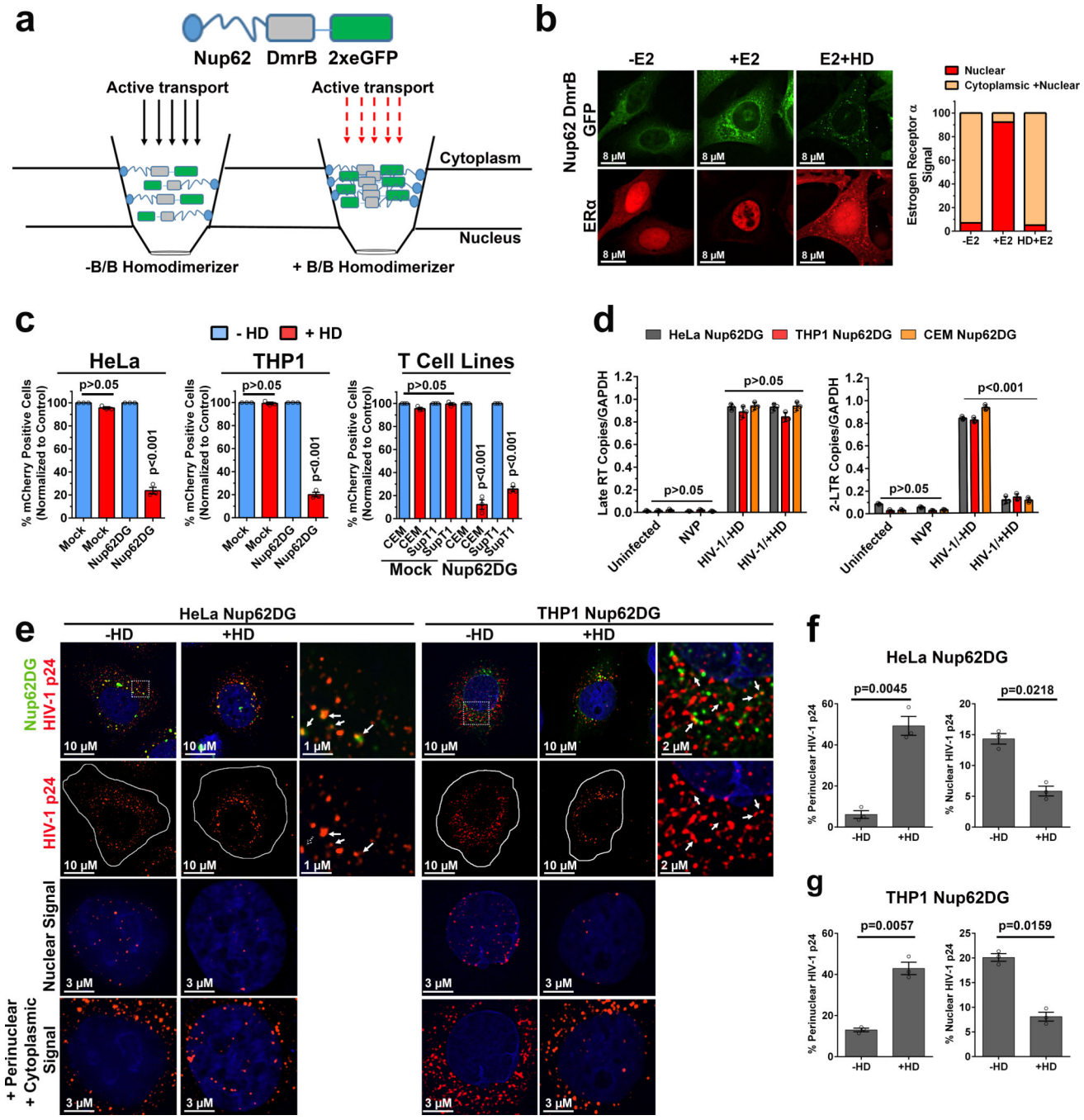

Figure 1: Artificial nuclear pore blockade inhibits HIV-1 infection at the nuclear entry stage.

a, Schematics of the Nup62 construct fused to the dimerization domain (DmrB) and 2 copies of eGFP (Nup62DG) used to block active nuclear pore transport after the addition of B/B homodimerizing drug (HD). **b**, HeLa cells were stably expressing the Nup62DmrBGFP construct and were transfected with estrogen receptor-α (ER-α) fused to mCherry. Twenty-four hours post-transfection, cells were treated with Estradiol (E2) for 30 min in the presence or absence of HD drug. Efficiency of nuclear pore blockade was quantified by counting cells having either nuclear ER-α signal (less efficient) or both nuclear and

cytoplasmic ER-α signal (efficient nuclear pore block). Data shown here is representative of three independent experiments. **c**, Mock or Nup62DG transduced HeLa, THP-1 differentiated macrophages, CEM and SupT1 T cells were synchronously infected with VSVg pseudotyped R7ΔEnvmCherry in the presence or absence of HD drug for the first 24 h of infection. HD drug removed after 24 h, was replaced with normal media and infection was assessed 48 h post synchronized infection by measuring the percent of mCherry positive cells. Shown normalized and averaged data (±SEM) from three independent experiments. **d**, q-RTPCR quantification of reverse transcription and 2-LTR circles in cells expressing Nup62DG, 24h following HIV-1 infection. Depicted mean of biological triplicates (±SD). Data shown here is representative of three independent experiments. **e**, HeLa and THP1 differentiated macrophages that stably express the Nup62DG construct were synchronously infected with VSVg-R7ΔEnvmCherry. Cells were treated with HD drug for 4 h, then fixed, and stained for HIV-1 capsid protein, p24, (red) and DAPI (blue) for cell nucleus. Colocalization between Nup62DG with p24 (boxed region) depicted by arrows **f**,**g** A quantification process was employed to detect perinuclear and nuclear p24 protein levels as described in the methods and extended data Fig 2. 20 or more cells analyzed in each experiment. Data averaged (±SEM) from three independent experiments. Statistical significance was assessed using Two-way ANOVA and Bonferroni post test. $P<0.05$ was considered significant in our experiments.

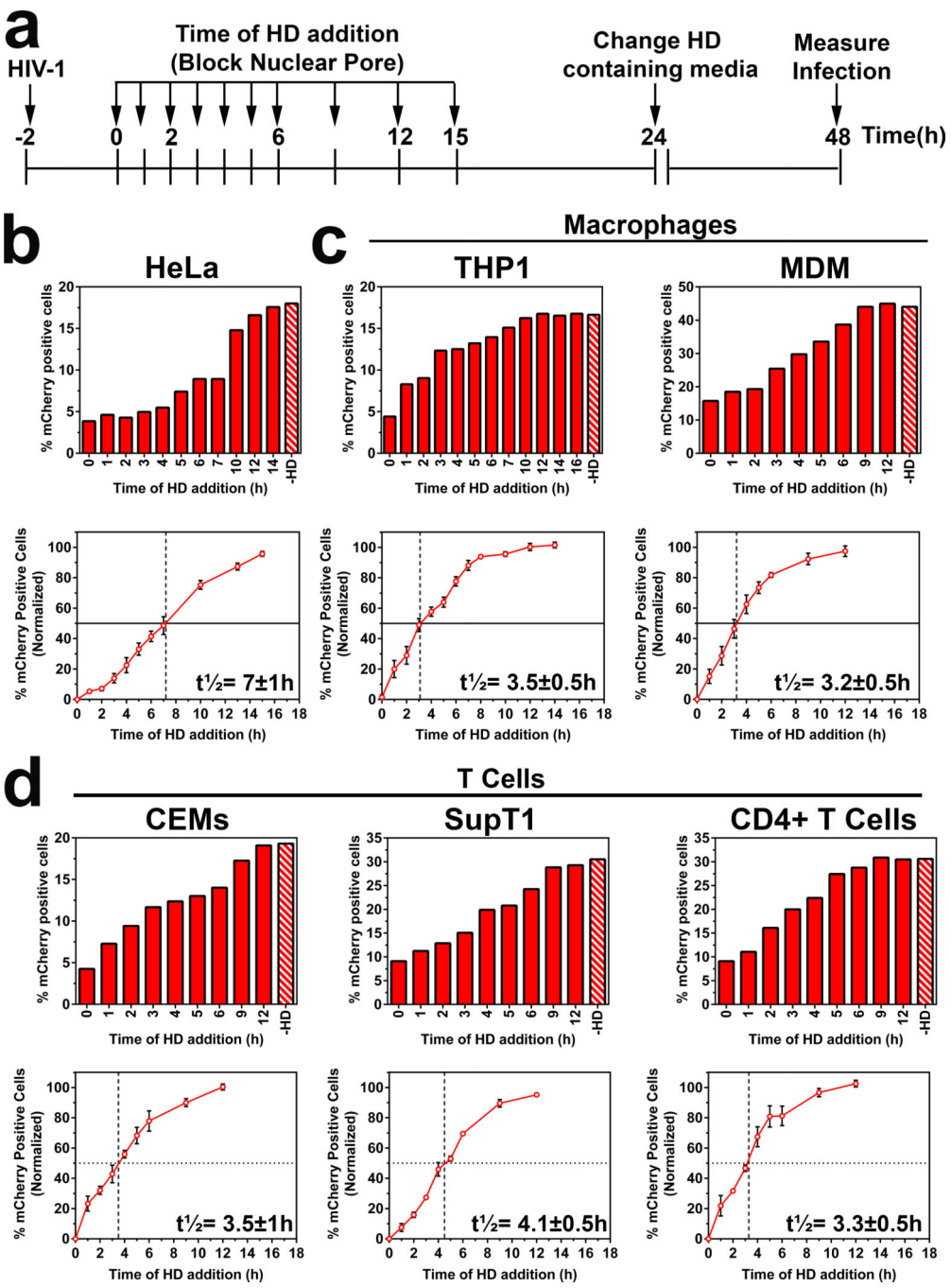

Figure 2: Monitoring HIV-1 nuclear import kinetics (NIK) reveals faster nuclear import in macrophages and T cells compared to HeLa cells.

a, Schematic of how nuclear import kinetics (NIK) were monitored in primary human macrophages, CD4+ T cells and various cell lines expressing the Nup62DG construct. Cells were synchronously infected with VSVg-R7ΔEnvmCherry for 2 h at 13°C before addition of HD drug to block nuclear pore import. HD drug was added at different time points post infection. Cells were incubated with HD until 24 h post-infection and then washed and replaced with normal media. Cells were harvested and infection was monitored by

measuring the percentage of mCherry positive cells 48 h post synchronized infection by flow cytometry. For monocyte derived macrophages (MDM), infection was monitored at 96 h. **b-d**, NIK were monitored in HeLa, THP-1 differentiated macrophages, primary monocyte derived macrophages (MDM),T cell lines, CEM and SupT1, and primary CD4+ T cells. Bar graphs depict data from a single experiment and line graphs depict normalized and average data (±SEM) from three independent experiments. Data were normalized by setting the baseline (0%) as the maximum inhibition attained by blocking the nuclear pore for 24 h (0h time point) and maximum infection (100%) as the infection attained with no HD treatment (dashed bars). Half time of NIK (t½) was shown in the line graph

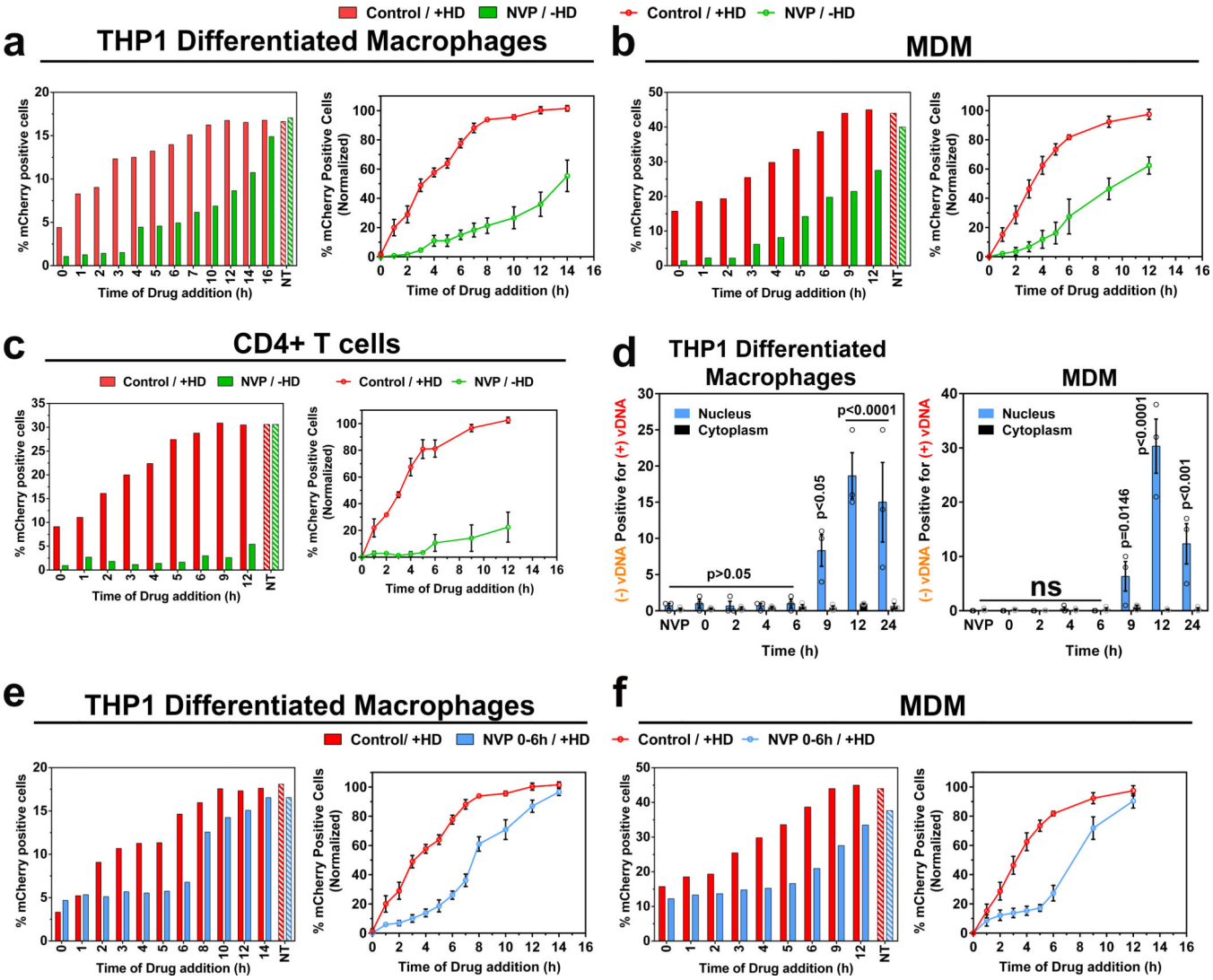

Figure 3: HIV-1 reverse transcription is required for efficient nuclear import and completes in the nucleus of the infected cell.

a–c, THP-1 differentiated macrophages (a) primary human macrophages (b) and primary CD4+ T cells (c) expressing the Nup62DG construct were infected with VSVg-R7ΔEnvmCherry and NIK was monitored by HD addition (red) as described in Fig 2. To monitor replication kinetics, the HIV-1 reverse transcriptase inhibitor, Nevirapine (NVP, 5μM), was added at different times post-infection as depicted (green) and was washed off at 24 h. Infectivity was measured as described in Fig 2. Bar graphs represent data from a single experiment and line graphs represent normalized and average data (±SEM) as described in Fig 2 from three independent experiments. **d**, The presence of HIV-1 nucleic acids in the nucleus of THP-1 differentiated macrophages and primary human macrophages was monitored. Cells were infected with VSVg-R7ΔEnvmCherry and were fixed at different time points post synchronized infection. Cells were treated with RNase A and stained for (−) vDNA and (+) vDNA using specific sense and antisense probes. Graph depicts the average number of (−) vDNA positive for (+) vDNA inside the nucleus from three independent experiments. 20 or more cells were analyzed in each experiment. Error bars represent the

SEM from three independent experiments. **e-f**, THP-1 differentiated macrophages (e) and primary human macrophages (f) expressing the Nup62DG construct were infected with VSVg-R7ΔEnvmCherry and NIK was monitored following HD addition alone (red) or in the presence of NVP treatment for the first 6 h (blue) following synchronized infection. Bar graphs represent data from a single experiment and line graphs represent normalized and average data (±SEM) as described in Fig 2 from three independent experiments. Statistical significance was assessed using Two-way ANOVA and Bonferroni post test. $P<0.05$ was considered significant in our experiments.

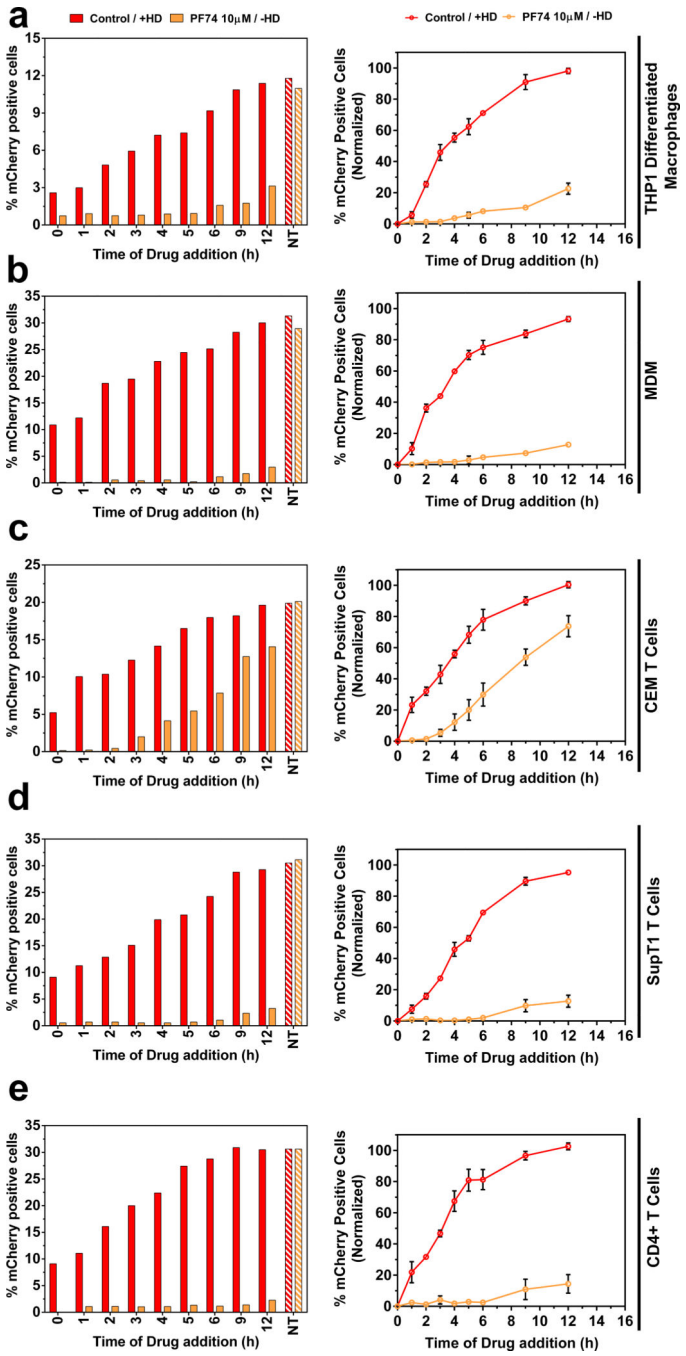

Figure 4: Nuclear HIV-1 capsid is required for productive infection.

a-e, Cells expressing the Nup62DG construct were infected with VSVg-R7ΔEnvmCherry and NIK were monitored following HD addition (red) as described in Fig 2. To disrupt assembled capsids, cells were incubated with 10 μM PF74 at different time points post synchronized infection as depicted (orange) and was washed off at 24 h. Infectivity was measured as described in Fig 2. Bar graphs represent data from a single experiment and

line graphs represent normalized and average data (±SEM) as described in Fig 2 from three independent experiments. NT represents no treatment.